

Detection of Single Nanoparticles inside a Single Terahertz Resonator

Young-Mi Bahk, Kyoung-Ho Kim, Gangseon Ji, Kwang Jun Ahn, Dai-Sik Kim, and Hyeong-Ryeol Park*

With the rapid advancement of 5G/6G communications using millimeter wavelengths, the concomitant usage of these long wavelength radiation for remote sensing and monitoring of biological and chemical agents is anticipated. However, the ability to detect and identify these agents with sizes ranging from nanometers to microns is hampered by its millimeter wavelength, which drastically reduces the interaction cross-section. Herein, it is reported that single gold nanoparticles (NPs) drop-casted on the nanoresonator can be observed by monitoring the far-field transmitting spectra of individual terahertz (THz) nanoresonators, which enhance the electric field hundreds of times on the nanoscale. Despite the enormous mismatch in length scales, full-wave 3D numerical modeling of the single THz nanoresonator is also performed to interpret the experimental results, indicating the possibility to turn off the resonance using only one NP embedded in the hotspot of the nanoresonator. Such NP detection becomes the most sensitive when the particle, whose size is comparable to the gap width, is tightly fitted into the nanoresonator. This work unveils the potential associated with refractive index sensing and hyperspectral absorption spectroscopy for detecting and fingerprinting ultra-low density of bio/chemical molecules such as viruses, lipid vesicles, and explosives.

NPs and biomolecules. In particular, THz frequency regime (0.1-30 THz) provides us with the low-frequency intra- and inter-molecular vibration information of chemical and biological molecules, such as explosives,^[6,7] deoxyribonucleic acid/ribonucleic acid molecules,^[8-10] polycrystalline glycines,^[11] glucose,^[12,13] and steroid hormones.^[14,15] However, THz sensing still remains a significant challenge due to poor coupling efficiency between the sub-millimeter wavelengths and nanometer-sized molecules. It has been recently demonstrated that engineered metamaterials, such as split ring resonators (SRRs), nanoresonators, and slot antennas, further improved the sensitivity for detecting trace amounts of target molecules enabled by the advancement of field enhancement and confinement on nanoscale.^[16-24] Although single nano-barriers, rods, and islands artificially fabricated on the array of THz nanoresonators were studied in earlier works,^[25-27] detection and sizing of drop-casted NPs on individu-

ally addressable nanoresonators are still needed to develop innovative sensing applications for viruses.^[28,29]

Here, we investigate whether single metal NPs with dimensions of 100 and 250 nm naturally attached to the gap of a single nanoresonator with a gap width of 120 nm can be detected using a THz wave with sub-millimeter wavelengths (Figure 1a,b). For detecting single NPs as promised by the strong field enhancement inside a single THz nanoresonator, we designed a single THz nanoresonator with a large length/width ratio of about 1250,

1. Introduction


Observation of single nanoparticles (NPs), having dimensions in the deep sub-wavelength region, has been still a big issue since it requires detection of very weak light absorption or scattering. The ability to detect individual NPs using sub-wavelength metallic structures, such as plasmonic dipole antennas,^[1,2] nanoapertures,^[3] microresonator,^[4] and plasmonic nanotubes,^[5] has been a widely spread tool for observing optical properties of single metal

Y.-M. Bahk
Department of Physics
Incheon National University
Incheon 22012, South Korea

K.-H. Kim
Department of Physics and Research Institute for Nanoscale Science and Technology
Chungbuk National University
Cheongju 28644, South Korea

G. Ji, D.-S. Kim, H.-R. Park
Department of Physics
Ulsan National Institute of Science and Technology
Ulsan 44919, South Korea
E-mail: nano@unist.ac.kr

K. J. Ahn
Department of Energy Systems Research
Ajou University
Suwon 16499, South Korea

 The ORCID identification number(s) for the author(s) of this article can be found under <https://doi.org/10.1002/adpr.202200134>.

© 2022 The Authors. Advanced Photonics Research published by Wiley-VCH GmbH. This is an open access article under the terms of the Creative Commons Attribution License, which permits use, distribution and reproduction in any medium, provided the original work is properly cited.

DOI: 10.1002/adpr.202200134

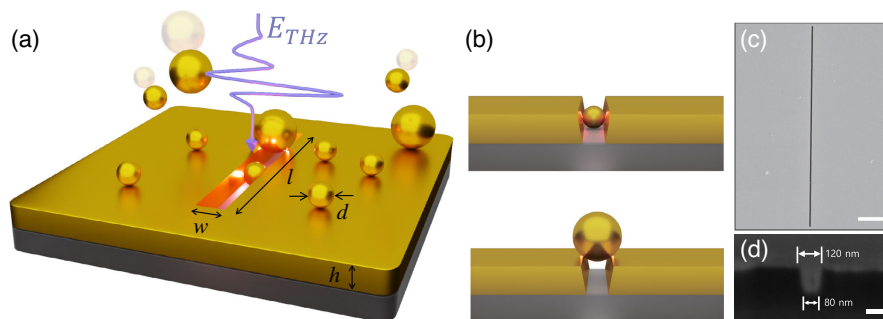


Figure 1. A single terahertz (THz) nanoresonator perturbed with single gold nanoparticles (NPs). a) Schematic of gold NPs with a size (d) placed on a single THz nanoresonator with a length (l) and a width (w) on a gold film with a thickness (h). b) Schematic of the gold NPs with (top) $d = 100$ nm “inside” and (bottom) $d = 250$ nm “on” the nanoresonator. c,d) Top and cross-sectional views of scanning electron microscope (SEM) image for a single THz nanoresonator with $l = 150$ μm and $w = 120$ nm on a gold film of $h = 100$ nm. Length of scale bars: c) 20 μm , d) 100 nm.

to have three orders of magnitudes of electric field enhancement.^[16,25,26] The resonance frequency of a single nanoresonator satisfies the condition $f_{\text{res}} = c/(2ln_{\text{eff}})$, where n_{eff} is the effective index of refraction of the composite of nanoresonator and substrate and l is the long-axis length of the nanoresonator.^[16] Using a focused ion beam machine, we fabricated a single nanoresonator suitable for our experimental purposes as shown in Figure 1c,d. Indeed, compared to the larger NPs (Figure 1b, bottom), the gap-sized gold NPs (Figure 1b, top) tightly embedded in the THz nanoresonator, which is a kind of slot antenna, induce a noticeable modulation of the THz transmission through the slot. This ability would pave a new way for improving the sensitivity for detection of NPs using nanogap-based metamaterials in infrared and THz regimes.

2. Results

To investigate THz responses of single nanoresonators, we performed THz time-domain spectroscopy (THz-TDS) in a frequency range from 0.3 to 2 THz using a femtosecond Ti:Sapphire laser with an 80 MHz repetition rate and 780 nm center wavelength. A single cycle THz pulse is generated from a biased low temperature-grown GaAs photoconductive antenna irradiated with the femtosecond laser and guided by two parabolic mirrors and two THz lenses as shown in Figure 2a. The electric field of THz pulse transmitted through the sample is detected via electro-optic sampling method using a $\langle 110 \rangle$ -oriented 1 mm-thick ZnTe crystal. To detect a tiny signal of transmission through a single THz nanoresonator with a coverage ratio of about 0.001%, we added the Tsurupica lens (invented by RIKEN) to the THz-TDS setup for tightly focusing THz wave. These THz lenses helped us to decrease the spot size at the focal point to below 1 mm, enhancing the THz electric field amplitudes by one order of magnitude compared with that of our old THz setup using the parabolic mirror only, while maintaining the signal-to-noise ratio of 10 000:1.

Figure 2b shows the measured THz time traces of single nanoresonators with a length of $l = 150$ μm and five different widths of $w = 120$ (red), 240 (orange), 500 (green), 1000 (blue), and 5000 nm (purple) for the p -polarized incident THz waves. While the single cycle pulses were measured from the

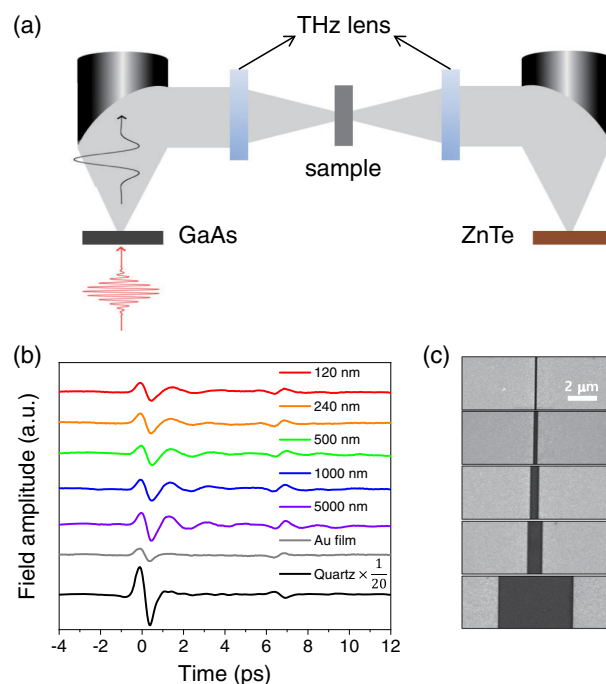


Figure 2. THz time-domain spectroscopy (THz-TDS) for monitoring a single THz nanoresonator. a) Schematic of THz-TDS setup using two parabolic mirrors and two Tsurupica THz lenses for a tight focusing of THz beam with 1 mm diameter at the sample position. b) Time traces of transmitted THz pulses through single THz nanoresonators with a length of $l = 150$ μm and different widths of 120 (red), 240 (orange), 500 (green), 1000 (blue), and 5000 nm (purple) and through the un-patterned gold film ($h = 100$ nm) (gray) and bare quartz (black). The time signals are offset along the vertical axis for clarity. It is noted that the black solid line for the bare quartz is scaled down 20 times for ease of comparison. c) Corresponding scanning electron microscope (SEM) images of the THz nanoresonators with different widths.

un-patterned 100 nm-thick gold film (gray) and bare quartz substrate (black), the oscillation behavior due to the strong resonant modes was observed in the single THz resonators. Also, as increasing the gap width from 120 to 5000 nm (Figure 2c), the period of second oscillation in the time domain becomes

shorter, which implies that the resonance frequency of a single THz nanoresonator shifts toward a higher frequency.

When incident electromagnetic waves resonantly couple to the metal gap structure, the electric field is strongly confined and enhanced in the gap, which results in a high transmission in the far field. By applying the Kirchhoff integral formalism, we extracted the near field enhancement factors quantitatively from the normalized transmitted amplitude ($t = E_{\text{sample}}(\omega)/E_{\text{ref}}(\omega)$) divided by gap-to-area coverage ratio (β), t/β , as shown in **Figure 3a**.^[30,31] $E_{\text{sample}}(\omega)$ and $E_{\text{ref}}(\omega)$ are the far-field amplitudes transmitted through the sample (THz resonators) and reference (bare substrate) obtained by Fourier transformation of the time-domain signal, respectively. As expected in the time-domain data, the electric field enhancement increases up to 722 at the redshifted resonance peak as decreasing the gap width to the narrowest scale, 120 nm.

While the experimental challenge of monitoring a single THz nanoresonator is addressed via tight-focusing of the THz beam, accurate computational modeling of THz wave propagation through the 150 μm long and 120 nm wide resonator poses another significant challenge. The enormous mismatch in length scales, up to 4 orders of magnitude between millimeter-scale wavelength and a hundred nanometer-scale width, was beyond the capabilities of commercial finite-difference time-domain or finite element methods (FEM). With 10 times improvement of DRAM chip capacity during the past 10 years, we employed a multi-scale meshing method based on the physical origin of the resonance to calculate full 3D field distributions and transmission spectra for the whole structure using a commercial FEM solution (see Experimental Section for the details). To double-check the electric field enhancements in the single THz nanoresonators, the gap widths of the top surface of the nanoresonator were 120, 240, 500, 1000, and 5000 nm, and the corresponding width of the bottom surface were 80, 200, 460, 960, and 4960 nm, considering the tapered geometry of the fabricated nanoresonators as shown in **Figure 1d**. The field enhancement was defined by E_{slot}/E_0 where E_{slot} is the average electric field on the top surface of the nanoresonator, and E_0 is the incident electric field on the same surface. **Figure 3b** shows

the estimated field enhancement spectra of the same THz nanoresonators used in **Figure 3a**. The simulated results in **Figure 3b** are in good quantitative agreement with the experimental data shown in **Figure 3a**.

Compared to the results of analytical calculations based on modal expansion with a single THz nanoresonator assuming a perfect electric conductor^[7,32–34] (see **Figure S1**, Supporting Information), the field enhancement spectra show higher peak enhancement factors than those of the simulation data, and, on the contrary, the peak frequency shifts to lower frequency with the decrease of the gap width. It is noteworthy that the redshift behavior is explained only with the calculations including a real metal effect,^[33] which indicates the significant effect of the gap plasmon mode on the resonance due to the penetrating electric field in the gold film. In addition, the field enhancement at the resonance frequency in the single THz nanoresonator is inversely proportional to the gap width, which is attributed to the increase of the capacitive charge accumulation in the gap region. The accumulated charges are distributed in a metal film within a length scale of gap size (w) from the metal edges, which results in a $1/w$ -dependent enhancement factor in this regime of $w > h$ (**Figure 3c**).

THz nanoresonators facilitate a strong interaction between millimeter waves and nano-sized objects such as NPs and nanowires. The experimental observations of the light–matter interaction are resonance shifts and transmission/reflection changes of the resonators. In the case of an array structure, the ensemble average interaction effects are observed because the configurations of each resonator element and NPs are randomly formed, even though the signal could be excellent in terms of sensing applications. However, monitoring a single structure, where the configuration of the resonator and NPs is exactly defined, allows us to further understand the resonant behaviors of each nanoresonator, strongly depending on the size and position of the NPs.

To investigate the THz response of a single nanoresonator perturbed by gold NPs, we coated the NPs with two different sizes of $d = 100$ and 250 nm on the single nanoresonators with

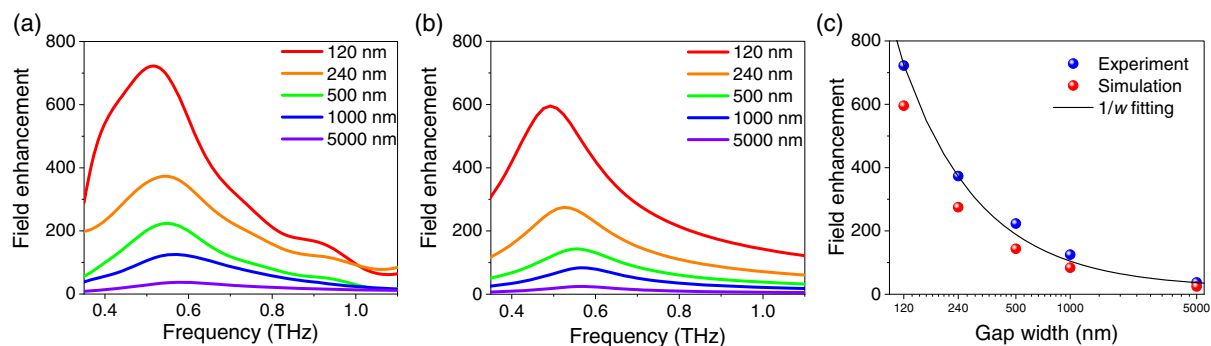


Figure 3. THz field enhancement spectra of the single THz nanoresonators. a) Measured THz electric field enhancement spectra through the single THz nanoresonators with a length of $l = 150 \mu\text{m}$ and widths of $w = 120$ (red), 240 (orange), 500 (green), 1000 (blue), and 5000 nm (purple) on a gold film with a thickness of $h = 100 \text{ nm}$. b) Calculated THz electric field enhancement spectra of the same THz nanoresonators used in **Figure 3a**. c) Maximum THz field enhancements of the experiments (blue) and the simulations (red) as a function of the gap width. The fitted solid line for blue dots denotes a $1/w$ dependence, where w is the gap width of the THz nanoresonator.

the same gap size of $w = 120$ nm using a drop-casting method (see the Experimental Section for the details of sample preparation). In Figure 4a,c, the two different sizes of NPs are located inside and over the metal gap, respectively, which results in two different perturbations on the resonant excitation of the metal nanostructure. With the gap-sized NPs ($d < w$), the transmitted amplitude is reduced by 33% relative to that of the resonator only through embedding only two NPs in the gap. Eventually, the resonance completely disappears with hundreds of NPs in the gap (Figure 4b). The number of NPs was counted in the corresponding SEM image right after measuring the THz transmittance (see Figure S2a,b, Supporting Information). This implies that a few gap-sized NPs could strongly disturb the fundamental resonant mode of the nanoresonator by acting as an obstacle despite the particle size being about 6,000 times smaller than the wavelength. In Figure 4c,d with the larger NPs ($d > w$), only 9% transmission reduction was counterintuitively observed, and the resonance peak does not disappear even with hundreds of NPs on the gap (see Figure S2c,d, Supporting Information). The small change in the transmission is attributed to the fact that the NPs, being practically attached to the gap, partially disturb the charge accumulation at two metal edges across the gap.

Furthermore, when the particle size is smaller than the gap size ($d < w$), a little transmission reduction is also obtained even with many NPs inside the gap (see Figure S3, Supporting Information), being consistent with the previous works using the array of THz slot antennas.^[21,24] It is worth noting that there is no significant change in transmission spectra when a billion of NPs or even more without the resonator are put onto a bare quartz substrate (Figure 4e,f).

Even though further studies are required to ensure the underlying physics, we deliberately suggest a possible origin. As the NPs become smaller, many contact points that possess resistive natures could be formed. Correspondingly, turning off the resonant transmittance is incompletely obtained because a current loss induced by the resistive contacts appears. This observation implies that an ideal sensitivity of the metal gap antenna structure strongly depends on the relative size of the gap and the refractive index of the target particles. The size-dependent perturbation of NPs disturbing the resonance of the THz nanoresonator can be explained by mimicking a resistor–inductor–capacitor (RLC) circuit model where the NPs are considered as additional resistors in parallel (Figure 4g,h). The surface current induced by the incident electromagnetic waves contributes

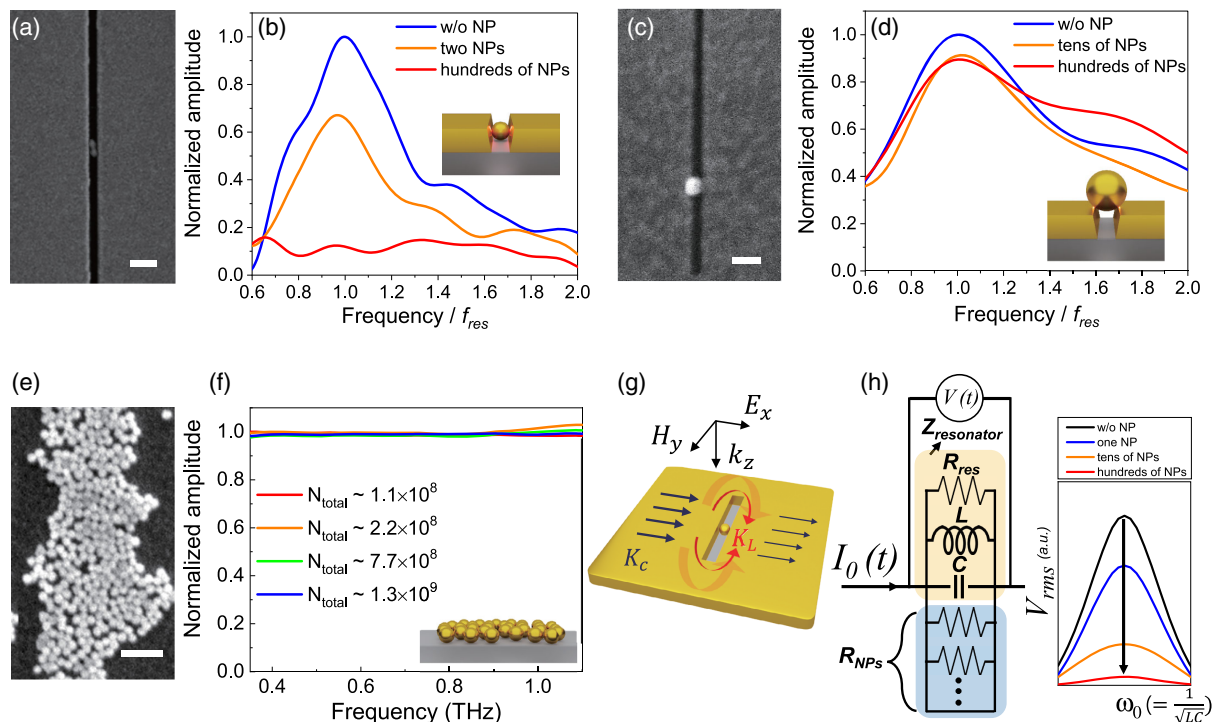


Figure 4. Single THz nanoresonators with gold NPs. a) Enlarged SEM image of the two gold NPs with $d = 100$ nm embedded in the 120 nm wide gap. b) Normalized transmitted amplitude spectra through single THz nanoresonators with $l = 150$ μm and $w = 120$ nm with (orange) the two and (red) hundreds of gold NPs, and (blue) without. c) Enlarged SEM image of the gold NPs with a diameter of $d = 250$ nm on top of the 120 nm wide gap. d) Normalized transmitted amplitude spectra through single THz nanoresonators with $l = 300$ μm and $w = 120$ nm with (orange) tens of and (red) hundreds of gold NPs, and (blue) without. e) Enlarged SEM image of the gold NPs with a total number of 1.3×10^9 on the bare quartz substrate. f) Normalized transmitted amplitude spectra for NP amounts ranging from 1.1×10^8 to 1.3×10^9 onto the bare substrate. g) An illustration of a single THz resonator with a gold NP where the surface current is induced in a metal film by an incident THz field. The induced current contributes to capacitive charging (K_C) and inductive coupling (K_L). h) (left) A distributed RLC circuit model for the single nanoresonator perturbed by gold NPs. The impedance of a single nanoresonator Z_0 is given by $[1/R_{\text{res}} - 1/(i\omega L) - i\omega C]^{-1}$. The NPs are responsible for an additional resistance R_{NP} in the circuit, resulting in (right) the lower Q factor of the rms voltage curve. Scale bars (all): 500 nm.

to a capacitive charging (K_C) and an inductive coupling (K_I) in the metal nanoresonator, resulting in resonant behavior (Figure 4g). The NPs disturbing the resonant mode play a role as an additional resistor leading to the lower Q factor at the resonance of $\omega_0 = 1/\sqrt{LC}$ (Figure 4h), which can imply the reduction of THz resonant transmission caused by the NPs. The capacitance $C = \epsilon_0 h/w$ is determined by the geometrical parameters where ϵ_0 is vacuum permittivity, h is metal thickness, l and w are the length and width of the resonator, respectively, and the inductance L can be extracted from the resonance frequency $f_{res} (= 1/(2\pi\sqrt{LC}))$ and the capacitance C .

With the wave impedance definition, we can estimate the NPs resistance R_{NP} that causes current loss. Consider the case for the size of NPs comparable to gap width ($d-w$) as shown in Figure 4b. The ratio of transmitted amplitudes for the resonator with and without NPs is expressed as $t_{NP}/t_0 = |Z_{NP}/Z_0|$ for transverse magnetic (TM) mode.^[35,36] At the resonance frequency, the effective impedances can be expressed by $Z_{NP} = [1/R_{res} + N/R_{NP}]^{-1}$ and $Z_0 = [1/R_{res}]^{-1}$ in terms of the resistance connected in parallel, where N is the number of NPs in the gap. For that case when two NPs exist in the gap as shown in Figure 4a, the ratio of transmitted amplitudes is around $t_{NP}/t_0 = 0.67$, which leads that the effective resistance of a single NP (R_{NP}) is around 4.1 times larger than the resistance for the resonator without NPs (R_{res}). The value is enough to significantly disturb THz resonant mode. In contrast, the larger NPs ($d > w$) have a much larger resistance due to the relatively small current loss through the NPs, determined by smaller electric field distributions above the gap.

In terms of the current flow through the metal NPs, according to previous works, it is expected that the NPs larger than the skin depth of the metal result in great perturbation with disturbing the charge accumulations.^[25,26] However, the use of metallic NPs changes both the size and contact resistance of the current flow channel depending on the particle size due to the different particle positioning (inside or above the gap). For gold NP larger than the skin depth, the currents pass through the NPs with a large effective resistance due to the small current loss.

To elucidate the physical origin of the perturbed resonance by a single gold NP, we calculated field enhancement spectra of the single THz nanoresonators with the gold NPs using the FEM calculation (see the Experimental Section for the details). The resonance of the single THz nanoresonator can be affected by the size and the position of the gold NP in the resonator. Indeed, we used the gold NP with a diameter of 100 nm fitted in the gap as shown in Figure 5a,c. The field enhancement was significantly suppressed when the single gold NP was placed at the center of the long-axis length of the resonator (red line in Figure 5a), meanwhile, the field enhancement was less suppressed when the gold NP has shifted 40 μm apart from the center of the resonator (orange line in Figure 5a). We note that these features become relatively much weaker when we put the larger gold NP with a diameter of 200 nm for the same positions (Figure 5b,d). In Figure 5c,d, the enhanced conducting current through the NP effectively turns off the resonance, reflecting most of the light back and achieving orders of magnitudes larger extinction when the NP is fitted into the gap rather than placed onto the top of the gap.

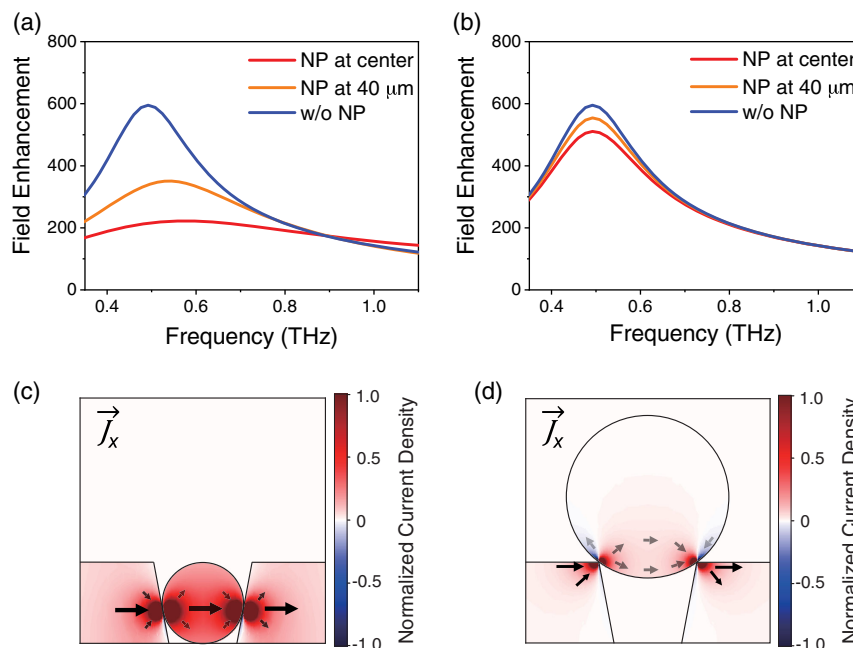


Figure 5. a,b) Calculated field enhancement spectra of a single THz nanoresonator with (red and yellow line) and without the single gold NP (blue line), using the FEM simulation. The gap width at the top surface of the nanoresonator was 120 nm. (a) The NP with a diameter of 100 nm was placed inside the gap region, and (b) the NP with a diameter of 200 nm was placed on top of the gap. The NPs were placed at the center (red lines) and 40 μm (orange lines) from the center of the 150 μm -long resonator. c,d) Normalized current density (J_x) distributions with: (c) the 100 nm NP embedded in the gap and (d) the 200 nm placed on top of the gap. Both of the NPs are located at the center of the long-axis length of the resonator. The black arrows describe the directions of the conducting currents through the NPs in the cross-sectional view. The current density J_x is normalized to the maximum value of each figure.

These results indicate two interesting features of the perturbed resonance by a single gold NP. First, the size of the gold NP is crucial for changing the resonance. The gap plasmon mode with the focused electric field in the gap region is the key to determining the resonance.^[37] The resonator with the 100 nm gold NP shows the larger suppression of the resonant transmittance compared to the one with the 200 nm gold NP, indicating the larger disturbance of the gap plasmon mode by the gold NP embedded inside the gap. The induced volumetric current inside the NP also supports that the 100 nm gold NP can severely affect the gap plasmon resonance by a resistive loss (Figure 5c,d). Furthermore, the electric field distributions in the single THz nanoresonator directly show the severe mode distortions by the 100 nm gold NP placed at the 40 μm from the center as well as at the center of the resonator (See Figure S4a, Supporting Information). In contrast, the electric field distributions with the 200 nm gold NP show subtle changes in the resonant modes because of the weak interaction with the gap plasmon mode (See Figure S4b, Supporting Information). Second, the perturbation of the resonance is a function of the position of the gold NP. The electric field distribution of the fundamental resonance shows a maximum at the center of the resonator. Therefore, the mode distortion by the NP is reduced when the NP moves toward the edge of the resonator. These results confirm that the perturbation of the resonance can be tuned by placing the NP at the desired position in the resonator, as already reported in the earlier works.^[25,26] Taken together, the 3D numerical simulations have confirmed that only a single gold NP can completely tune the resonance of the THz nanoresonator, enabling the development of an ultrasensitive THz sensing platform for various conducting and non-conducting NPs, such as viruses and lipid vesicles with diameters of less than 100 nm.^[24,38–40]

3. Conclusions

We have demonstrated the detection and sizing of drop-casted metal NPs on individually addressable nanoresonators in the THz frequency region. The dramatic THz transmission change was realized only when the size of the gold NP is comparable to the gap size, which results from strongly perturbing the fundamental resonant mode of the nanoresonator. Intrinsically, the only one NP with a diameter of 100 nm could shut off the resonant transmittance through the 150 μm -long nanoresonator despite the particle's dimension being smaller than about $\lambda_{\text{res}}/6,000$. This phenomenon is attributed to the presence of the strong field enhancement and confinement inside the nanogap, which could increase the scattering or the absorption from NPs thereby enabling the detection of subwavelength particles beyond the diffraction limit. Besides the detection of NPs, our nanoresonator platform can be also utilized to study various sensing applications for bio/chemical molecules due to their spectral selectivity in a wide range from the mid-infrared to the THz region, where their resonance responses can be tuned to that of the intra- and intermolecular vibrational modes of target molecules. This sensing platform will lead to a great impact on the advancement of fingerprinting ultra-low density of explosives and viruses, especially if this platform is combined with trapping techniques.^[24,41]

4. Experimental Section

Optical Simulations: The full-wave optical simulations were performed to analyze the field enhancement of the single THz nanoresonators in Figure 3 and the nanoresonators with a gold NP in Figure 5, using a finite-element method (COMSOL Multiphysics, RF module). The nanoresonator was formed by perforating a rectangular hole in the 100 nm-thick gold film with the dielectric constant following the Drude model, $\epsilon(\omega) = 1 - \omega_p^2 / (\omega^2 + i\omega\gamma_p)$ with the ω_p of 2730 THz and the γ_p of 19.4 THz.^[7,42] The length of the THz nanoresonator was 150 μm and the gap widths of the top surface of the nanoresonator were 120, 240, 500, 1000, and 5000 nm and their corresponding width at the bottom surface were 80, 200, 460, 960, and 4960 nm by considering the tapered geometry of the fabricated nanoresonator in Figure 1d. The thin gold film area was extended to 1 mm from the edge of the nanoresonator for considering the lambda-zone with the surface current flow.^[43] The gap region and the top layer of the nanoresonator were air, and the bottom side was the quartz substrate with a refractive index of 2.0.

The different length scales in the gap width (120 nm), the length of the THz nanoresonator (150 μm), and the wavelength (600 μm at 0.5 THz) demand huge amounts of computational resources such as memories and CPUs. To resolve it, we applied a multi-scale meshing method based on the physical origin of the resonance in the THz nanoresonator. The largest element size in free space is 55 μm whereas the smallest element size in the gap is 5 nm. The focused Gaussian beam with the beam waist of 500 μm was used to model the focused THz light illuminating the nanoresonator from air. The outer boundary of the calculation region was set to be the perfectly matched layer to eliminate the unwanted reflection. The non-local effect was not considered in the simulation due to ohmic contacts between the NP and the nanoresonator.

Sample Preparation: A drop-casting method was used for coating the gold NPs. We used colloidal gold NPs with sizes of 100 nm and 250 nm (EM.GC 100/4 and EM.GC 250/4, BBI solutions). We dropped the 10 μL (Figure 4b, orange) and 20 μL colloidal solutions (Figure 4b, red) on the single nanoresonators, and subsequently dried the sample at a room temperature of 20 $^\circ\text{C}$. The volume density of the 100 nm gold NP colloidal solution was $5.5 \times 10^9/\text{mL}$. Therefore, the total number of gold NPs over the entire area of the sample can be estimated to be 5.5×10^7 (for the 10 μL solution) and 1.1×10^8 (for the 20 μL solution), respectively. The total number of 250 nm gold NPs was also estimated in the same manner.

Supporting Information

Supporting Information is available from the Wiley Online Library or from the author.

Acknowledgements

Y.-M.B., K.-H.K., and G.J. contributed equally to this work. This work was supported by the National Research Foundation of Korea (NRF) grant funded by the Korean government (NRF-2015R1A3A2031768, NRF-2018R1A2B6001449, NRF-2019R1C1C1006681, NRF-2021R1A2C1008452, NRF-2022R1A2C1011655), the Republic of Korea's MSIT (Ministry of Science and ICT), under the High-Potential Individuals Global Training Program (Task No. 2021-0-01580) supervised by the IITP (Institute of Information and Communications Technology Planning & Evaluation), and 2022 Research Fund (1.220061.01 and 1.190098.01) of Ulsan National Institute of Science and Technology (UNIST)

Conflict of Interest

The authors declare no conflict of interest.

Author Contributions

Y.-M.B., G.J., K.J.A., D.-S.K., and H.-R.P. conceived and designed the experiments, and K.-H.K. performed the numerical simulations. All authors analyzed the data and wrote the manuscript together.

Data Availability Statement

The data that support the findings of this study are available from the corresponding author upon reasonable request.

Keywords

drop-casting method, focused ion beam, nanogap antennas, single nanoparticles, terahertz nanoresonators, terahertz sensing, terahertz time-domain spectroscopy

Received: May 3, 2022

Revised: July 7, 2022

Published online: August 17, 2022

-
- [1] M. Righini, P. Ghenuche, S. Cherukulappurath, V. Myroshnychenko, F. J. G. de Abajo, R. Quidant, *Nano Lett.* **2009**, *9*, 3387.
- [2] W. H. Zhang, L. N. Huang, C. Santschi, O. J. F. Martin, *Nano Lett.* **2010**, *10*, 1006.
- [3] R. Gordon, *Adv. Opt. Mater.* **2020**, *8*, 2001110.
- [4] J. Zhu, S. K. Ozdemir, Y.-F. Xiao, L. Li, L. He, D.-R. Chen, L. Yang, *Nat. Photonics* **2010**, *4*, 46.
- [5] J. McPhillips, A. Murphy, M. P. Jonsson, W. R. Hendren, R. Atkinson, F. Hook, A. V. Zayats, R. J. Pollard, *Acs Nano* **2010**, *4*, 2210.
- [6] J. S. Melinger, N. Laman, D. Grischkowsky, *Appl. Phys. Lett.* **2008**, *93*, 011102.
- [7] H.-R. Park, K. J. Ahn, S. Han, Y.-M. Bahk, N. Park, D.-S. Kim, *Nano Lett.* **2013**, *13*, 1782.
- [8] M. Nagel, P. H. Bolivar, M. Brucherseifer, H. Kurz, A. Bosserhoff, R. Buttner, *Appl. Opt.* **2002**, *41*, 2074.
- [9] B. M. Fischer, M. Hoffmann, H. Helm, R. Wilk, F. Rutz, T. Kleine-Ostmann, M. Koch, P. U. Jepsen, *Opt. Express* **2005**, *13*, 5205.
- [10] S. H. Lee, J. H. Choe, C. Kim, S. Bae, J. S. Kim, Q. H. Park, M. Seo, *Sens. Actuators B Chem.* **2020**, *310*, 127841.
- [11] Y. Shi, L. Wang, *J. Phys. D: Appl. Phys.* **2005**, *38*, 3741.
- [12] K. Lee, K. Jeoung, D. K. Lee, Y. B. Ji, M. Seo, Y. M. Huh, J. S. Suh, S. J. Oh, *Infrared Phys. Technol.* **2018**, *93*, 154.
- [13] C. Song, W. H. Fan, L. Ding, X. Chen, Z. Y. Chen, K. Wang, *Sci. Rep.* **2018**, *8*, 8964.
- [14] A. A. Angeluts, A. V. Balakin, M. G. Evdokimov, M. N. Esaulkov, M. M. Nazarov, I. A. Ozheredov, D. A. Sapozhnikov, P. M. Solyankin, O. P. Cherkasova, A. P. Shkurinov, *Quantum Electron.* **2014**, *44*, 614.
- [15] S. H. Lee, D. Lee, M. H. Choi, J. H. Son, M. Seo, *Anal. Chem.* **2019**, *91*, 6844.
- [16] H. R. Park, Y. M. Park, H. S. Kim, J. S. Kyoung, M. A. Seo, D. J. Park, Y. H. Ahn, K. J. Ahn, D. S. Kim, *Appl. Phys. Lett.* **2010**, *96*, 121106.
- [17] S. J. Park, B. H. Son, S. J. Choi, H. S. Kim, Y. H. Ahn, *Opt. Express* **2014**, *22*, 30467.
- [18] S. J. Park, J. T. Hong, S. J. Choi, H. S. Kim, W. K. Park, S. T. Han, J. Y. Park, S. Lee, D. S. Kim, Y. H. Ahn, *Sci. Rep.* **2014**, *4*, 4988.
- [19] D.-K. Lee, J.-H. Kang, J.-S. Lee, H.-S. Kim, C. Kim, J. Hun Kim, T. Lee, J.-H. Son, Q. H. Park, M. Seo, *Sci. Rep.* **2015**, *5*, 15459.
- [20] W. D. Xu, L. J. Xie, J. F. Zhu, X. Xu, Z. Z. Ye, C. Wang, Y. G. Ma, Y. B. Ying, *Acs Photonics* **2016**, *3*, 2308.
- [21] Y.-S. Ryu, D.-K. Lee, J.-H. Kang, S.-H. Lee, E.-S. Yu, M. Seo, *Opt. Express* **2017**, *25*, 30591.
- [22] Y. M. Bahk, D. S. Kim, H. R. Park, *Adv. Opt. Mater.* **2019**, *7*, 1800426.
- [23] M. Seo, H.-R. Park, *Adv. Opt. Mater.* **2020**, *8*, 1900662.
- [24] E. S. Yu, S. H. Lee, G. Lee, Q. H. Park, A. J. Chung, M. Seo, Y. S. Ryu, *Adv. Sci.* **2021**, *8*, 2004826.
- [25] H. R. Park, Y. M. Bahk, K. J. Ahn, Q. H. Park, D. S. Kim, L. Martin-Moreno, F. J. Garcia-Vidal, J. Bravo-Abad, *Acs Nano* **2011**, *5*, 8340.
- [26] H. R. Park, Y. M. Bahk, J. H. Choe, S. Han, S. S. Choi, K. J. Ahn, N. Park, Q. H. Park, D. S. Kim, *Opt. Express* **2011**, *19*, 24775.
- [27] M. Seo, J. H. Kang, H. S. Kim, J. H. Cho, J. Choi, Y. M. Jhon, S. Lee, J. H. Kim, T. Lee, Q. H. Park, C. Kim, *Sci. Rep.* **2015**, *5*, 10280.
- [28] S. J. Park, S. H. Cha, G. A. Shin, Y. H. Ahn, *Biomed. Opt. Express* **2017**, *8*, 3551.
- [29] D.-K. Lee, J.-H. Kang, J. Kwon, J.-S. Lee, S. Lee, D. H. Woo, J. H. Kim, C.-S. Song, Q. H. Park, M. Seo, *Sci. Rep.* **2017**, *7*, 8146.
- [30] M. A. Seo, H. R. Park, S. M. Koo, D. J. Park, J. H. Kang, O. K. Suwal, S. S. Choi, P. C. M. Planken, G. S. Park, N. K. Park, Q. H. Park, D. S. Kim, *Nat. Photonics* **2009**, *3*, 152.
- [31] J. S. Kyoung, M. A. Seo, H. R. Park, K. J. Ahn, D. S. Kim, *Opt. Commun.* **2010**, *283*, 4907.
- [32] F. J. Garcia-Vidal, E. Moreno, J. A. Porto, L. Martin-Moreno, *Phys. Rev. Lett.* **2005**, *95*, 103901.
- [33] F. J. Garcia-Vidal, L. Martin-Moreno, E. Moreno, L. K. S. Kumar, R. Gordon, *Phys. Rev. B* **2006**, *74*, 153411.
- [34] J. H. Kang, J. H. Choe, D. S. Kim, Q. H. Park, *Opt. Express* **2009**, *17*, 15652.
- [35] S. Han, J.-Y. Kim, T. Kang, Y.-M. Bahk, J. Rhie, B. J. Kang, Y. S. Kim, J. Park, W. T. Kim, H. Jeon, F. Rotermund, D.-S. Kim, *Acs Photonics* **2016**, *3*, 1440.
- [36] A. Calabrese, D. Gacemi, M. Jeannin, S. Suffit, A. Vasanelli, C. Sirtori, Y. Todorov, *Nanophotonics* **2019**, *8*, 2269.
- [37] J. Jeong, D. Kim, M. Seo, D. S. Kim, *Nano Lett.* **2019**, *19*, 9062.
- [38] R. H. Olsen, J. S. Siak, R. H. Gray, *J. Virol.* **1974**, *14*, 689.
- [39] M. H. Woo, Y. M. Hsu, C. Y. Wu, B. Heimbuch, J. Wander, *J. Aerosol Sci.* **2010**, *41*, 944.
- [40] Y. M. Bar-On, A. Flamholz, R. Phillips, R. Milo, *Elife* **2020**, *9*, 57309.
- [41] R. Gordon, *Opt. Laser Technol.* **2019**, *109*, 328.
- [42] M. A. Ordal, L. L. Long, R. J. Bell, S. E. Bell, R. R. Bell, R. W. Alexander, C. A. Ward, *Appl. Opt.* **1983**, *22*, 1099.
- [43] J. H. Kang, D. S. Kim, Q. H. Park, *Phys. Rev. Lett.* **2009**, *102*, 093906.